PNAS RESEARCH ARTICLE | IMMUNOLOGY AND INFLAMMATION
BIOPHYSICS AND COMPUTATIONAL BIOLOGY

T cell and B cell antigen receptors share a conserved core transmembrane structure

Samyuktha Ramesh[a,b], Soohyung Park[c,d,e], Wonpil Im[c,d,e], Melissa J. Call[a,b,1,2], and Matthew E. Call[a,b,1,2]

Edited by Ian Wilson, The Scripps Research Institute, La Jolla, CA; received May 16, 2022; accepted October 6, 2022

The B cell and T cell antigen receptors (BCR and TCR) share a common architecture in which variable dimeric antigen-binding modules assemble with invariant dimeric signaling modules to form functional receptor complexes. In the TCR, a highly conserved T cell receptor αβ (TCRαβ) transmembrane (TM) interface forms a rigid structure around which its three dimeric signaling modules assemble through well-characterized polar interactions. Noting that the key features stabilizing this TCRαβ TM interface also appear with high evolutionary conservation in the TM sequences of the membrane immunoglobulin (mIg) heavy chains that form the BCR's homodimeric antigen-binding module, we asked whether the BCR contained an analogous TM structure. Using an unbiased biochemical and computational modeling approach, we found that the mouse IgM BCR forms a core TM structure that is remarkably similar to that of the TCR. This structure is reinforced by a network of interhelical hydrogen bonds, and our model is nearly identical to the arrangement observed in the just-released cryo-electron microscopy (cryo-EM) structures of intact human BCRs. Our biochemical analysis shows that the integrity of this TM structure is vital for stable assembly with the BCR signaling module CD79AB in the B cell endoplasmic reticulum, and molecular dynamics simulations indicate that BCRs of all five isotypes can form comparable structures. These results demonstrate that, despite their many differences in composition, complexity, and ligand type, TCRs and BCRs rely on a common core TM structure that has been shaped by evolution for optimal receptor assembly and stability in the cell membrane.

B cell receptor | antigen receptor | transmembrane | receptor structure | receptor assembly

Significance

Lymphocyte antigen receptors are modular biosensors that detect the presence of pathogen-derived molecular fragments. The T cell receptor (TCR) assembles via polar/electrostatic interactions within the membrane and is built around an evolutionarily conserved core structure formed by the ligand-binding TCRαβ transmembrane (TM) domains. We now show that the ligand-binding membrane immunoglobulin (mIg) TM domains in the B cell receptor (BCR) form a core structure that is strikingly similar to that of the TCR and plays a crucial stabilizing role in the assembled receptor. A TM helix–association motif that forms part of this interface has been used and reused in immune receptors throughout evolution, pointing to a previously unappreciated level of TM structural conservation in antigen receptors and related proteins.

B and T lymphocytes utilize antigen receptor complexes at their cell surfaces, known as the B cell receptor (BCR) and the T cell receptor (TCR), respectively, to generate signals that orchestrate lymphocyte development and direct adaptive immune responses. These receptor complexes are each composed of an antigen-binding module with no intrinsic signaling capability that noncovalently associates with one or more signaling modules containing immunoreceptor tyrosine-based activation motifs (ITAMs) that initiate intracellular biochemical cascades upon phosphorylation (1, 2) (Fig. 1 *A* and *B*). The BCR contains a membrane-bound immunoglobulin (mIg) for antigen binding, which is an alternatively spliced form of a secreted antibody with a C-terminal transmembrane (TM) domain and short cytoplasmic domain (3, 4). The mIg is associated with the CD79AB signaling dimer (also known as Igαβ) (5, 6) (Fig. 1*A*) to form the complete receptor complex. The TCR is an octameric complex consisting of either a TCRαβ or γδ subunit for antigen binding, which is reminiscent of a membrane-tethered antibody Fab (7–9), and three signaling dimers, namely CD3δε, CD3γε, and ζζ (10–15) (Fig. 1*B*). The TCR, like most other modular activating receptors, assembles its components through basic and acidic residues in the TM domains of the antigen-binding and signaling subunits, respectively (10–17) (Fig. 1 *B* inset). However, the BCR TM domains lack these matched electrostatic contacts, and what type of TM interactions drive its assembly has long been an open question.

The first structure of a single-pass receptor complex in which the TM interactions were well resolved was of a human αβ TCR (9), enabled by recent advances in cryo-electron microscopy (cryo-EM) (Fig. 1*B*). Reflected in this structure is the intricate packing of the TCR's eight subunits within the membrane, organized around an extensive αβ TM interface at its core. This core structure was first identified by a combination of cysteine scanning, NMR spectroscopy, and molecular dynamics (MD) simulations (18) that generated a model (Fig. 1*C*) with a backbone Cα RMSD of only 0.63 Å with respect to the later cryo-EM structure (19), proving this methodology to be highly effective at obtaining structural information on challenging membrane-embedded receptors. Driven by highly conserved amino acids (Fig. 1 *C* and *D*) that form an interchain hydrogen bond network,

Author contributions: W.I., M.J.C., and M.E.C. designed research; S.R. and S.P. performed research; S.R., S.P., W.I., M.J.C., and M.E.C. analyzed data; and S.R., S.P., W.I., M.J.C., and M.E.C. wrote the paper.

The authors declare no competing interest.

This article is a PNAS Direct Submission.

[1]M.J.C. and M.E.C. contributed equally to this work.

[2]To whom correspondence may be addressed. Email: mjcall@wehi.edu.au or mecall@wehi.edu.au.

This article contains supporting information online at https://www.pnas.org/lookup/suppl/doi:10.1073/pnas.2208058119/-/DCSupplemental.

Published November 21, 2022.

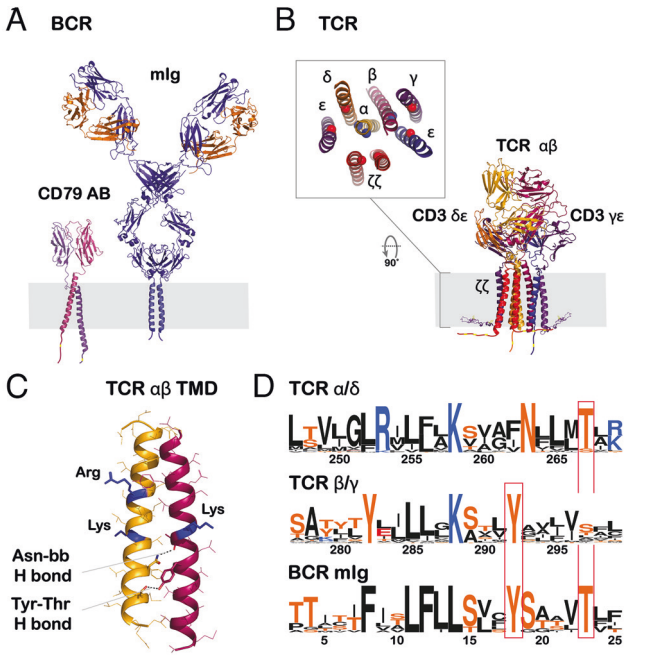

Fig. 1. The B and T cell antigen receptors share highly conserved Y and T residues in their antigen-binding subunit TM domains. (*A*) Components of the BCR complex: ligand-binding mIg and signaling CD79AB. Structures shown of mIgM extracellular domains are from PDB IDs 6KXS, 4JVU and 1ADQ, and CD79AB from Alphafold2 prediction. (*B*) Components of the TCR complex: ligand-binding TCRαβ and signaling CD3δε, CD3γε, and ζζ. PDB IDs: 6JXR human αβ TCR extracellular domains and TM domains, 2K4F CD3ε tail with ITAM tyrosines shown in yellow. *Inset*: top view of the TCR complex showing the TM domain with assembly-mediating basic (blue) and acidic (red) residues as spheres. Gray box around the TM domains represents the cell membrane. (*C*) TCR αβ TM model generated by experimentally restrained modeling (18) showing key polar interactions at the dimer interface. Assembly-mediating basic residues are colored blue. (*D*) Weblogos showing evolutionary conservation of the TM domain sequences of over 65 species of TCR αβ/γδ and all isotypes of mouse and human BCR mIgs. Polar uncharged residues are colored orange, basic residues in blue, and acidic residues in red. The highly conserved Y and T residues (boxed in red) found at the TCR αβ interface are also highly conserved and similarly spaced in mIg. TCR numbering is based on Dong et al. (9). BCR numbering starts from the beginning of its TM domain.

this interface is a critical determinant of TCR stability (18, 20). Sequence alignments and MD simulations indicate that this structure is also present in the γδ- and pre-TCR complexes across all vertebrate species that have conventional T cells (20).

It has long been recognized that antigen receptor TM domains contain a small number of amino acid positions that are conspicuously conserved not only among different TCR forms or mIg isotypes, but also between TCR and BCR proteins (21). In the absence of any structural information, clues to the role of these conserved residues in the BCR mIg TM domain came primarily from reports that mutations at some of these positions could disrupt BCR assembly and surface expression (22–27). Most previous models of the BCR in the membrane have therefore incorporated an assumption that the helical face of the mIg TM domain containing the most conserved amino acids forms direct contacts with the CD79 TM domains (28–31). However, we noted that some of the most conserved positions across mIg isotypes aligned well in sequence and spacing with key contacts across the recently described heterodimeric TCRαβ TM interface (9, 18, 20) (Fig 1*D*), particularly a tyrosine (Y) in TCRβ and a threonine (T) in TCRα that are encoded on the same chain in the homodimeric mIg to form a YxxxxT motif (where x is any amino acid). This motif also drives dimer formation in the TCR-associated ζζ module (32), the antibody Fc receptor-associated γγ module (33), and the T cell immunomodulatory receptors CD28 (34, 35) and cytotoxic T lymphocyte-associated protein 4 (CTLA-4) (34). We therefore set out to test whether the BCR mIg TM domains form a similar core structure to TCR via self-association of their conserved helical faces. Using an unbiased approach encompassing cysteine crosslinking, restrained MD simulations, and mutagenesis in a cell-free receptor assembly system, we found that these structures are indeed remarkably similar. We further show that all mIg isotypes can form the same dimeric interface and that its integrity is crucial for BCR assembly. Our model of the core TM structure from restraints collected in native B cell-derived ER membranes is in excellent agreement with the newly released cryo-EM structures of the full-length BCR in detergent micelles (36, 37).

Results

In Vitro Assembly of the BCR in ER Microsomes. The in vitro translation (IVT) system using nuclease-treated rabbit reticulocyte lysate is competent for protein synthesis when supplemented with mRNA encoding proteins of interest and amino acids (including ^{35}S-labeled methionine and cysteine for detection). With the addition of endoplasmic reticulum (ER) microsomes, numerous immune receptors (including the TCR) have successfully been assembled in this system (16–18, 38–41). However, assembly of the BCR has not previously been reported. Using affinity-tagged components of the BCR, we assembled a hen egg lysozyme (HEL)-specific murine IgM (HyHEL10) BCR (42) including κ light chain (LC, no tag), FLAG-tagged mIgM heavy chain (HC-FLAG), streptavidin-binding peptide-tagged CD79A(-SBP), and influenza hemagglutinin-tagged CD79B(-HA). Following cotranslational assembly in the ER microsomes, BCR complexes were extracted with digitonin to preserve noncovalent interactions and immunoprecipitated via the affinity tags either individually or sequentially (Fig. 2 *A* and *B*). BCRs were successfully assembled, as seen by the coimmunoprecipitation (IP) of all chains by each strategy. A control assembly in which mIg and CD79AB were assembled in separate reactions and combined just prior to digitonin extraction shows that BCR components that were not cotranslationally assembled in the same ER microsome did not associate (Fig. 2*A* starred (*) lane). The IVT system was therefore deemed suitable to perform a cysteine scan to identify positions that are in close proximity within the assembled BCR.

Cysteine Scanning Identifies Specific Crosslinks in the mIg TM Dimer. A library of mIgM mutants with single cysteine substitutions at every TM position was generated to perform the disulfide scanning. In initial experiments, treatment with the membrane-penetrating oxidizing agent copper (II) phenanthroline (CuPhe), which is required to catalyze intramembrane disulfide bond formation, caused a high background of misfolded products, presumably due to the large number of Ig domains present in the mIgM complex (five in each HC, two in each LC: 14 total). For this reason, we elected to use a previously reported HC truncation lacking the distal two HC Ig domains (Fig. 2*B*), which retains the ability to assemble with CD79 and express at the cell surface (43). This construct (HC^{trunc}) assembled efficiently with CD79 in IVT reactions, and a double cysteine mutant (C327S, C404S; C-less HC^{trunc}) ablated the native interchain disulfide bonds to allow readout of TM crosslinks as reappearance of a covalent HC homodimer (Fig. 2*C*).

A panel of 28 TM and tail cysteine mutants on C-less HC^{trunc} were assembled with CD79AB, oxidized with CuPhe, extracted with digitonin, and immunoprecipitated with either anti-FLAG beads (targeting HC^{trunc}) or a mix of streptavidin and anti-HA beads

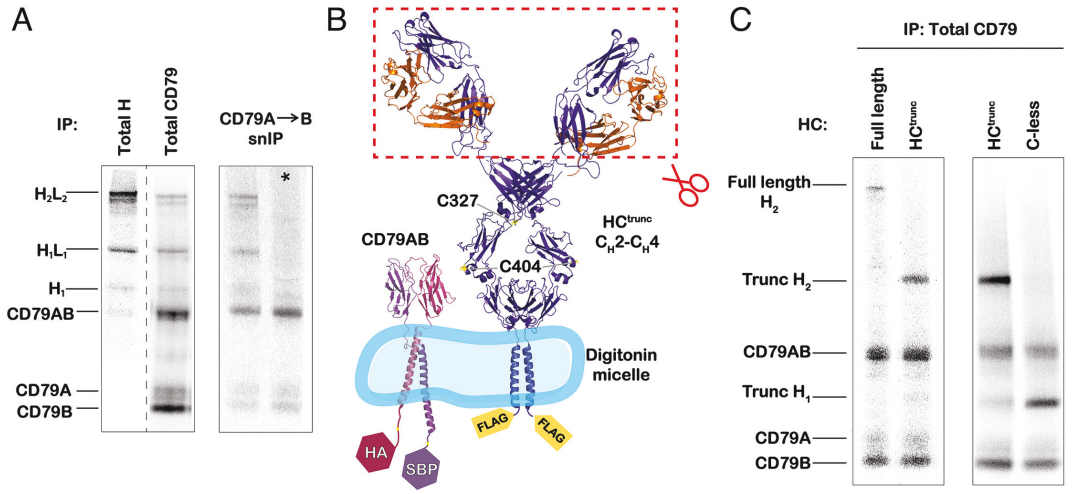

Fig. 2. In vitro assembly of the BCR complex in ER microsomes. (*A*) BCR mIg HC, CD79A, and CD79B were assembled by in vitro translation in ER microsomes for 4 h. The assembled complexes were extracted in 0.5% digitonin and immunoprecipitated targeting either the HC (anti-FLAG beads) or total CD79 (streptavidin and anti-HA beads) (*Left*). Samples were deglycosylated with Endo H and analyzed by nonreducing SDS-PAGE. Each IP strategy yielded all chains of the BCR, showing assembly of the complex. Alternatively, a sequential nondenaturing IP from CD79A to B (streptavidin to anti-HA) could purify CD79AB heterodimers and all associated BCR chains (*Right*). *: mixing control reaction where HC and CD79 chain mRNAs were added to separate IVT reactions and combined at the extraction step. The lack of co-IP of HC with CD79AB shows that only cotranslationally assembled BCR complexes survive the IP. (*B*) Schematic showing the BCR chains and their C-terminal affinity tags. The extracellular portion removed in the HC^{trunc} construct is boxed in red. The cysteines mutated to serines in the C-less construct are highlighted in yellow. (*C*) HC^{trunc} and C-less HCs are capable of assembling into BCR complexes comparable to WT. Complexes were assembled as described in (*A*).

(targeting total CD79). Samples were then deglycosylated and analyzed by nonreducing sodium dodecyl sulfate–polyacrylamide gel electrophoresis (SDS-PAGE). The IP targeting HC^{trunc} showed that most cysteine mutants were capable of forming crosslinked dimers, although the strength of dimerization varied widely across the positions (Fig. 3*A*). There was a clear helical periodicity seen in the extent of crosslinking at each consecutive TM position (summary plot in Fig. 3*E*), indicating the involvement of one specific face of the helix in dimerization. Only a fraction of these mutants, however, were capable of forming dimers that also coprecipitated with CD79 subunits (Fig. 3*B*). An even more stringent sequential IP that strictly isolates assembled CD79AB heterodimers (Fig. 3*C*) showed further selectivity for only a few cysteine mutants that formed crosslinked dimers in the context of defined mIg-CD79AB complexes, with L1C, A5C, and S19C being the strongest (numbered with respect to position in the TM domain). Visualizing these on a helix wheel diagram (Fig. 3*D*) shows that the strongest crosslinks lie on one face of a helix. Among these crosslinks, S19C is unique in that it associates with CD79AB almost exclusively in its crosslinked dimeric form. Combined data from these three analyses are shown together on a summary plot in Fig. 3*E*.

Some previous studies reported that resting BCRs exist as oligomers that may contain intercomplex TM contacts (30, 44–46). To ensure that the crosslinks identified here had formed between two HCs of one BCR complex, and not HCs of neighboring BCR complexes, we introduced the S19C mutation on the cysteine-sufficient HC^{trunc} (*SI Appendix*, Fig. S1). On this already-dimeric HC^{trunc} background, any additional TM crosslinks formed between neighboring BCRs would result in the formation of covalent oligomers ("daisy-chains") which should be visible by nonreducing SDS-PAGE (*SI Appendix*, Fig. S1 *B* and *C*). Assembly and crosslinking of this S19C on HC^{trunc} BCR did not result in detectable daisy-chains (*SI Appendix*, Fig. S1*D*), confirming that the S19C crosslink forms within one BCR complex. These experimentally derived proximity-mapping data show that a specific dimeric interface exists between the mIg HC TM domains within an assembled BCR complex and that this interface includes residues L1, A5, and S19.

Experimentally Guided Computational Assembly of the mIgM TM Dimer. The three positions that formed the strongest crosslinks (L1, A5, and S19) (Fig. 4*A*) were used as distance restraints to model the mouse mIgM TM domains, as previously done for the heterodimeric TCRαβ TM domains (18). A 7-ns replica exchange molecular dynamics (REMD) simulation was performed using the Generalized Born with a simple SWitching (GBSW) implicit membrane model (47) in Chemistry at Harvard Macromolecular Mechanics (CHARMM) (48) and converged on a single dominant cluster. The centroid model from this cluster showed a structure compatible with all the three strong crosslinks (Fig. 4*C*), with the Cβ–Cβ distances between the restraining pairs remaining at ~4 Å over the course of the simulation (Fig. 4*B*). This model showed that the surface of the mIgM TM helix containing the most conserved positions forms a complementary homodimer interface (Fig. 4*D*). This interface notably contains several polar residues that are well positioned to form interchain hydrogen bonds that could make significant contributions toward stabilizing the mIg homodimer within the membrane, specifically at S15–S15, S19–S19, and each Y18–T23 pair (Fig. 4*E*).

To exclude the possibility that the crosslink-derived distance restraints had enforced an unfavorable dimer interface during REMD assembly, we performed unrestrained MD simulations in fully atomistic 1-palmitoyl-2-oleoyl-sn-glycero-3-phosphocholine (POPC) bilayers using the above model as the starting structure. Five independent 500-ns simulations (total simulation time 2.5 μs) confirmed that the structure did not significantly deviate from the REMD model over the simulation period (Fig. 4*E*). Contact maps between all residues in the model and Cα RMSD over the simulation time with respect to the REMD model are available in *SI Appendix*, Fig. S2. Consistent with the small Cα RMSD (<2 Å) and strong contacts over the entire TM domain (*SI Appendix*, Fig. S2 *A* and *B*), the distances (d_{HH}) and crossing angles (Ω) between TM helices were steady around mean values (*SI Appendix*, Fig. S2 *C* and *D*), with a narrow distribution and a sharp peak around d_{HH} = 8 Å and Ω = 20° (*SI Appendix*, Fig. S2*E*). In addition, the interhelical Cα–Cα distances at residues 12 to 19 were not sensitive to Ω (*SI Appendix*, Fig. S2*F*), indicating that

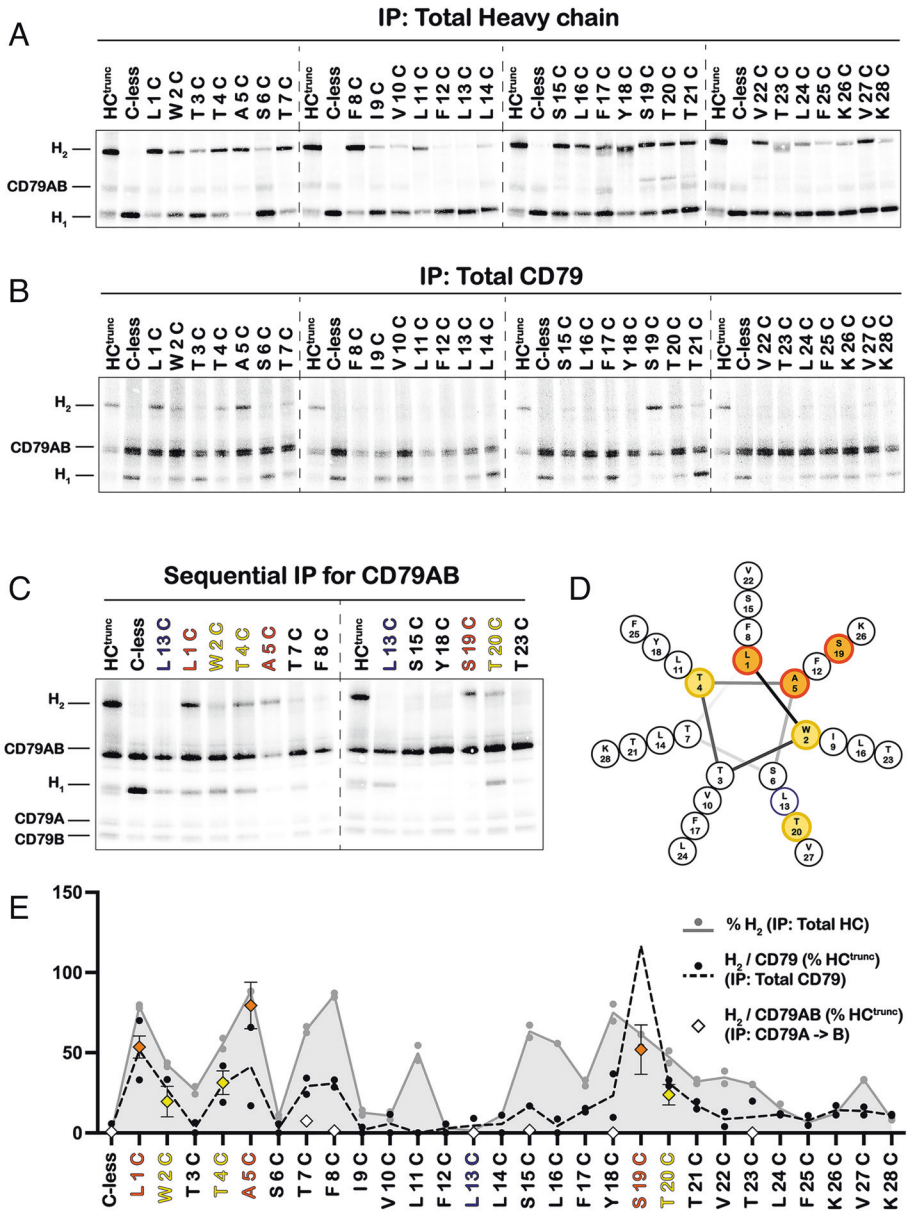

Fig. 3. Cysteine scanning of the mIg HC TM domain identifies highly specific crosslinks. (*A*–*C*) Cysteine mutants generated on the C-less HC^{trunc} background were assembled into BCR complexes by IVT for 4 h. Complexes were extracted in 0.5% digitonin and immunoprecipitated targeting (*A*) HC (anti-FLAG), (*B*) total CD79 (streptavidin and anti-HA), or (*C*) CD79AB (snIP from streptavidin to anti-HA). Samples were Endo H-treated and analyzed by nonreducing SDS-PAGE. Most cysteine mutants were able to form crosslinked dimers (*A*), while only a subset of them assembled with CD79 (*B*). These were further refined to three key cysteine mutants (orange) that formed strong dimers and also assembled with CD79AB heterodimers: L1C, A5C, and S19C (*C*). Weaker CD79AB-associated HC dimers are colored yellow. (*D*) Positioning of these strong (orange) and weak (yellow) crosslinks on a helix wheel diagram reveals a likely interaction face on the mIg HC TM helix. (*E*) Summary plot showing the helical periodicity of the crosslinks. Densitometry was performed on the experiments shown in panels *A*–*C* and the normalized yield of HC dimer was plotted. Solid gray line and gray dots: Yield of H_2 as a percentage of total H from total HC IP (representative autoradiogram in *A*); line traces the mean of N = 2 and dots show individual data points. Dashed black line and black dots: Yield of H_2 with respect to CD79A, as a percentage of HC^{trunc}. Calculated from total CD79 IP (representative autoradiogram in *B*); line traces the mean of N = 2 and dots show individual data points. Diamonds: Yield of H_2 with respect to CD79AB, as a percentage of HC^{trunc}. Calculated from sequential CD79A to B IP (representative autoradiogram in *C*); mean ± SD, N=3. Strongest, assembly-competent crosslinks are highlighted in orange and weaker crosslinks in yellow.

the TM dimer interface in this region is tight and well maintained. This is also supported by the hydrogen bond analysis (see Table 1), which showed a high probability of hydrogen bonds at S15–S15 (~91%) and Y18–T23 (~85%), with lower probability of S19–S19 (~38%) and S15–S19 (~34%) hydrogen bonds, suggesting that the mIgM TM dimer interface was indeed stabilized by hydrogen bonding involving at least some of these residues.

Close Packing of the mIg TM Dimer Is Necessary for BCR Assembly in the Membrane. To assess whether the close apposition of TM helices in the mIg dimer was required for BCR assembly, we introduced a series of aliphatic substitutions at the two serine positions (S15, S19) found at the packing interface (Fig. 5*A*). Mutations to alanine, valine, and leucine were made at each position on the full-length HC and the mutants were assembled with CD79AB by IVT (this assembly did not require a CuPhe treatment step). The assembled complexes were extracted in digitonin, immunoprecipitated via total CD79, deglycosylated, and analyzed by reducing SDS-PAGE to quantify the yield of HC relative to CD79 (Fig. 5 *B* and *C*). S15A and S15V mutations were clearly detrimental, indicating that the hydrogen bond is particularly important at this site. Interestingly, S15L was not disruptive, suggesting that leucine could make complementary packing interactions that overcome loss of the hydrogen bond, while valine and alanine could not (Fig. 5*C*). This site therefore requires either hydrogen bonding or close complementary packing for efficient assembly. In contrast, S19A was not detrimental to assembly, while S19V and S19L were showing that this site requires close packing but not necessarily hydrogen bonding (Fig. 5*C*). These results are consistent with the constant S19–S19 Cα–Cα distance and the lower probability of hydrogen bonds at S19 than S15 in the MD analysis above.

Complex Hydrogen Bonding Interactions Contribute to BCR Assembly in the Membrane. Using the same experimental setup, we next evaluated the effects of alterations at the Y18–T23 hydrogen bond pair using mutations that removed the polar hydroxyl groups while limiting additional changes to side-chain size and chemistry. We found that Y18F disrupted assembly, while T23V did not, and these two mutations together assembled with CD79 just as well as the WT sequence (Fig. 5*D*). This suggests that the Y–T hydrogen bond is dispensable, but leaving T23 without its partner leads to alternative interactions that do not support

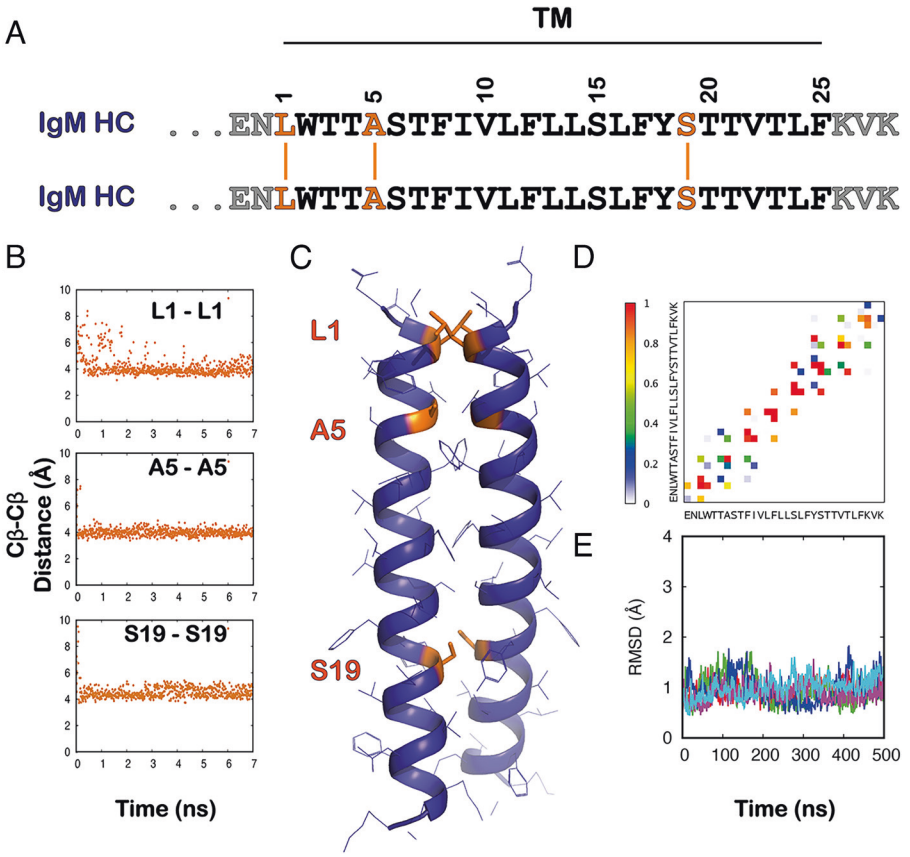

Fig. 4. Experimentally guided MD simulations reveal an mIgM TM dimer structure. (*A*) Sequence of mIgM HC TM domain with the strongest (orange sold lines) crosslinks identified. The strong crosslinks were used as distance restraints for REMD simulations. (*B*) Cβ–Cβ distances between the restraining residue pairs over the REMD simulation are maintained at ~4 Å. (*C*) REMD model of the mIgM TM dimer with positions of strongest crosslinks highlighted in orange. (*D*) Contact probability map between all modeled TM residues, averaged over the five replicas from the last 200 ns of the unrestrained simulations. Contacting residue pairs are defined as those within 4.5 Å heavy atom distance. (*E*) Cα RMSD between the unrestrained MD simulations and the mIgM REMD model over the indicated simulation time. Each of the five replicas are shown as different colors.

assembly. Combination of Y18F with the inert S19A mutation did not further exacerbate the assembly defect (Fig. 5*E*), but combination with S15A caused near-complete loss of assembly with CD79. This defect was even more severe than the loss of all interface hydrogen bonds simultaneously (S15A, Y18F, S19A, and T23V combined, termed "NoHB" in Fig. 5*E*), reinforcing the conclusion that partial disruptions can be more deleterious, possibly through alternative hydrogen bonding interactions that enforce unfavorable conformations.

BCR mIgM and TCRαβ TM Domains Form Very Similar Structures. Structural alignment of the BCR mIgM TM homodimer with the previously reported TCRαβ TM heterodimer reveals a remarkable degree of similarity (Fig. 6*A*), with backbone Cα RMSD of only 0.87 Å or 0.68 Å between mIgM and TCRαβ from the restrained simulations (18) or the subsequent cryo-EM structure (9), respectively. The hydrogen bonding network in the C-terminal (bottom) half of the mIg interface indeed bears a striking similarity to the polar network comprising TCRα N263, TCRα T267, and TCRβ Y292 that stabilizes the core of the TCR complex (18) (Fig. 6*B*), as we had hypothesized based on sequence alignments and conservation (see Fig. 1*D*). A similar pattern of Y–T hydrogen bonds contributes to dimer formation in other immune receptors including the TCR-associated ζ chain (32), the antibody Fc receptor-associated FcεR1γ subunit (33), and the T cell costimulatory and inhibitory receptors CD28 (34, 35) and CTLA4, respectively (34) (Fig. 6*C*). We therefore interrogated whether the Y–T contacts and the proximal serines at the mIgM packing interface contribute similarly to the stability of BCR complexes formed by other mIg isotypes.

All BCR Isotypes Are Compatible with the Conserved Core TM Domain Structure. We reasoned that if the TM dimer structure identified in mIgM was crucial for assembly with CD79AB to form an intact receptor, then mIgs of all the four additional BCR isotypes must be able to adopt stable structures mediated by a similar interface. To test this hypothesis, we performed MD simulations of mouse mIgD, mIgG, mIgA, and mIgE (Fig. 7*A*) in POPC bilayers (Fig. 7*B*), with each mIg sequence modeled on the mouse mIgM REMD backbone as the starting structures. Five independent 500-ns simulations were performed for each isotype, all of which maintained stable structures that did not depart significantly from the mIgM reference model over the simulation (Fig. 7*C*), with the exception of mIgD, which showed looser N-terminal packing. Contact maps between all residues

Table 1. Hydrogen bond occupancy (% ± SE)

Residue pair	mIgA	mIgD	mIgM	mIgG	mIgE
S/T15–S/T15	79 ± 18	0	91 ± 3	86 ± 7	45 ± 18
S19–S19	18 ± 4	50 ± 3	38 ± 7	41 ± 9	–
Y18–T23	89 ± 6	92 ± 2	88 ± 9	94 ± 4	98 ± 0
T23–Y18	57 ± 16	84 ± 12	82 ± 7	57 ± 17	98 ± 1
S/T15–S19	41 ± 8	0	47 ± 14	27 ± 9	–
S19–S/T15	7 ± 2	0	21 ± 12	21 ± 13	–

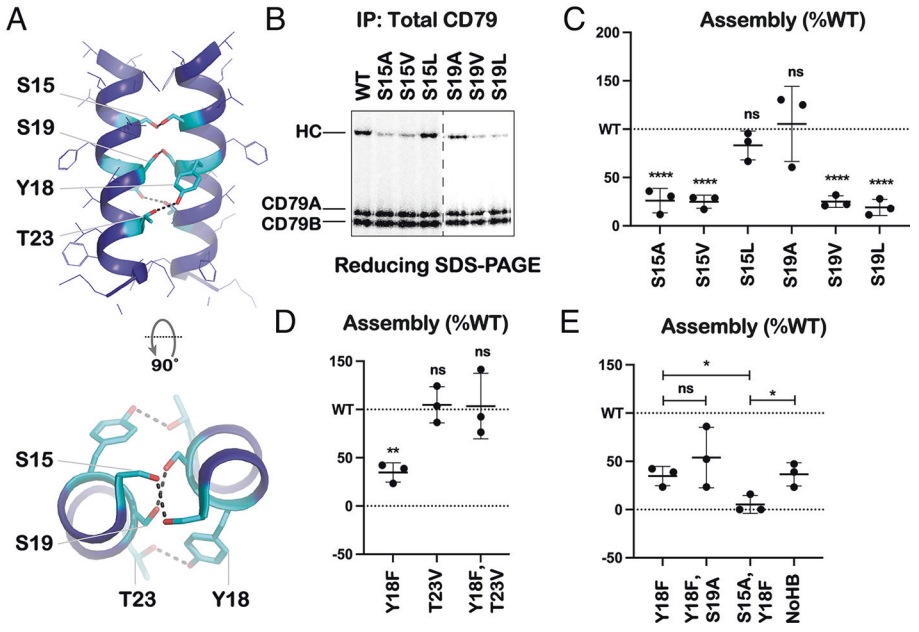

Fig. 5. Interactions at the mIg TM interface are crucial for stable BCR assembly. (*A*) *Top*: Side view of C-terminal end of the mIgM TM dimer with the residues involved in interfacial hydrogen bonding colored cyan. *Bottom*: Top-down view of the hydrogen bonding network. (*B–E*) The requirement for hydrogen bonding and/or close packing at the mIg TM interface for BCR assembly was tested with mutations that removed hydrogen bonding capability or increased steric bulk. Full-length HC proteins with the indicated mutations were assembled with CD79A and B by IVT. BCR complexes were extracted in digitonin and immunoprecipitated targeting total CD79 (simultaneous streptavidin and anti-HA capture). Samples were deglycosylated and analyzed by reducing SDS-PAGE. Representative autoradiogram is shown in (*B*). (*C* and *D*) Densitometry was performed on the autoradiograms and the yield of HC with respect to CD79A (as a percentage of WT) was plotted as a measure of assembly competence of the mutants. N = 3, error bars show SD, significance with respect to WT (*C* and *D*) or between the indicated mutants (*E*) calculated by RM one-way ANOVA with uncorrected Fisher's LSD test and single pooled variance, $*P < 0.05$, $**P < 0.01$, $***P < 0.001$, $****P < 0.0001$.

and Cα RMSD with respect to the mIgM REMD model over the simulations are shown in *SI Appendix*, Fig. S2. Though there are variations between isotypes, the core of the TM dimer interface was well maintained in all isotypes, which is also indicated by the constant F12–F12 and S19–S19 Cα–Cα distances.

The probability of Y18–T23 hydrogen bonding was very high for all isotypes (Fig. 7*D* and Table 1). Interestingly, both mIgA and mIgG showed some asymmetry in the Y18–T23 hydrogen bond occupancy on the opposite sides of the dimer (Table 1), and analysis of individual trajectories revealed that these side chains are bridged by a water molecule in some simulations (*SI Appendix*, Fig. S3). This suggests that there is some inherent propensity for asymmetry in the two Y18–T23 contacts when other polar ligands are available, which may bear relevance to how the mIg TM dimer interacts with CD79 on only one side (see *Discussion*). High occupancy was also observed for an additional hydrogen bond at T5–T5 in mIgA (Fig. 7*C* and Table 1), which is the only isotype with a polar residue at this position. This lies right at the dimer interface, in the same position as mIgM A5 that was one of the strongest cysteine crosslink positions (see Figs. 3 and 4). For mIgA and mIgG, the probability of hydrogen bonds was high at S15, as observed for mIgM. In mIgD, which has a threonine at position 15 instead of serine, no hydrogen bonding was seen at this position, likely due to the increased flexibility at the N-terminal end of the TM domain for this isotype and/or steric hindrance from tight packing below this site. In most simulations, S19 hydrogen bonds were less frequent but still significant, again similar to mIgM. The mIgE sequence contains glycine at position 19 instead of serine, so there is no hydrogen bond here. For the other isotypes, there was considerable occupancy of hydrogen bonds between S15 of one helix and S19 of the opposing helix, which are spaced one turn apart at the interface. Despite these minor differences, the overall architecture of all isotypes remained globally similar, particularly in the lower (C-terminal) half (Fig. 7*C*), supporting their adoption of a similar configuration to that determined experimentally for mIgM. Together with our previous reports on TCR TM structure (18, 20), these data demonstrate that this conserved core TM structure is found in all lymphocyte antigen receptors.

Discussion

Here, we have applied a combination of cysteine crosslinking, MD simulations, and mutagenesis to identify an interface in the BCR's mIg TM domain that is crucial to the stability of the receptor complex. The Y–T hydrogen bonds at this interface define a shared structural element in the BCR mIg and TCRαβ TM domains. The high degree of conservation at these positions between TCR and BCR has been previously noted (21), and we now provide experimental evidence that they encode a shared TM domain structure. While the two lymphocyte antigen receptors' similar genetic organization and mechanisms of gene rearrangement suggest that they originated from a gene duplication event

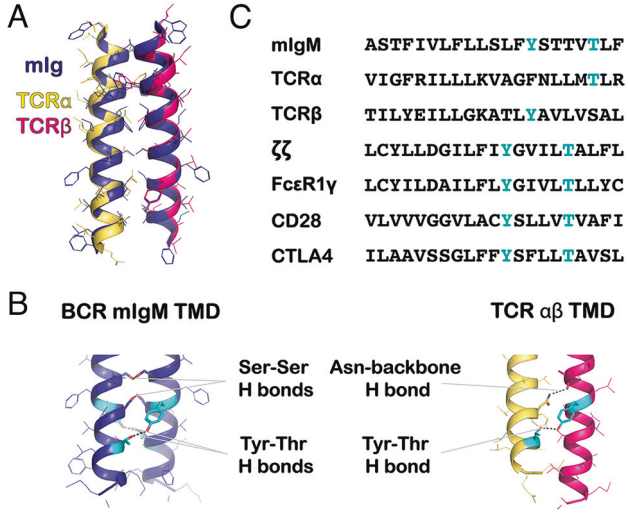

Fig. 6. BCR mIg and TCR αβ TM domains form highly similar dimeric structures. (*A*) Alignment of the TM domains of BCR mIgM (blue) and TCR αβ (yellow and pink, PDB ID: 6JXR (9)). Residues aligned: mIg W2-F25, TCRα N246-R269, TCRβ L276-L299, numbering based on Fig. 1. The backbone Cα RMSD between mIgM and TCRαβ TM domains is 0.68 Å. (*B*) Hydrogen bonding stabilizes the lower half of both interfaces, with the BCR mIg containing a polar network among Ser, Tyr, and Thr residues and TCR αβ containing a network involving Asn, Tyr, and Thr. The shared Y–T staple is highlighted in cyan. (*C*) Sequences of other immune protein dimers which are also stabilized by the Y–T staple (cyan).

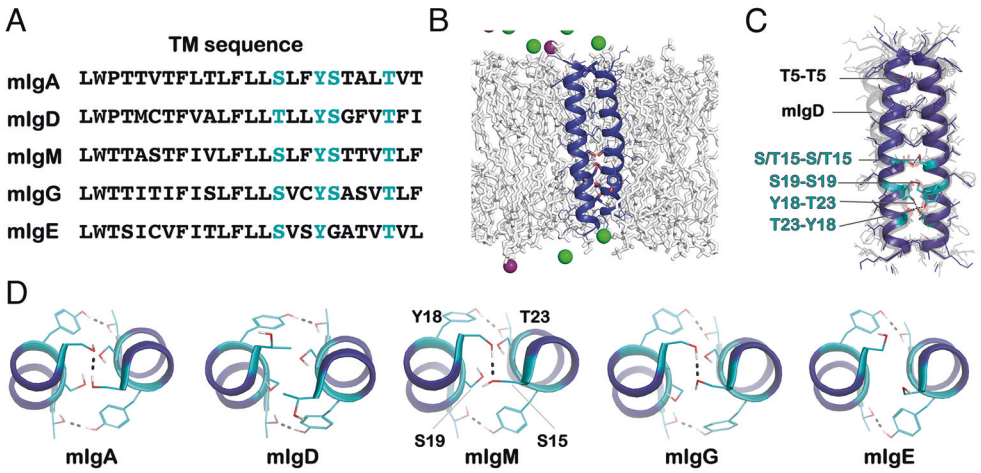

Fig. 7. BCR mIgs of all the five isotypes can form similar homodimeric TM structures. (*A*) TM domain sequences of the five mouse mIg isotypes. The residues involved in the mIg TM interfacial polar network are colored cyan. (*B*) Representative snapshot from the modeling of the mIg TM domains (blue) equilibrated in fully atomistic POPC bilayers (white) over five 500 ns simulations. Shown together are potassium (green) and chloride ions (purple). Water, hydrogen, and components in front of the mIg TM domains are omitted for clarity. (*C*) Overlay of the structures adopted by the five mIg isotypes (gray) with respect to the mIgM REMD model (blue, used to define backbone Cα starting coordinates for all isotypes). Most isotypes formed structures highly similar to mIgM, with only mIgD showing some looser packing at the top end. Interfacial Ser, Tyr, and Thr polar network residues are colored cyan. The position of T5 in mIgA, where an additional hydrogen bond was seen, is also indicated. (*D*) Top-down view of the polar network interactions in the five mIg isotypes based on the hydrogen bond occupancy analysis (Table 1).

(49–53), the many differences in their molecular organization and activity, including the number of subunits, the mechanism of assembly, and the mode and sensitivity of antigen engagement, render this commonality in their TM architecture an unexpected finding.

Previous models of BCR TM arrangement had the most conserved mIg helical face mediating assembly with CD79, specifically with both Y18 and S19 acting as direct and requisite CD79 contact points (23, 26–29). However, our results clearly demonstrate that neither of these positions make *requisite* CD79 contacts because both the S19A single mutant and the Y18F/T23V double mutant were well tolerated (see Fig. 5). Furthermore, the mIgM dimer stabilized by an S19C-mediated disulfide bond still associated well with CD79 (see Fig. 3), showing that the structure with S19 buried in the homodimer interface is assembly competent. While this manuscript was in revision, two groups published cryo-EM structures of intact human BCR complexes (36, 37) that confirm our model and inform on how the mIg TM homodimer assembles with CD79 in the membrane. Our mouse mIgM TM model aligns to the corresponding region of the higher-resolution human mIgM structure 7XQ8 (37) with a backbone RMSD of just 0.57 Å and makes all of the same interface contacts (*SI Appendix*, Fig. S4 *A–C*). While our model is fully symmetrical, the cryo-EM structure shows a small departure from symmetry that puts Y18 on one side of the dimer in close proximity to a potential hydrogen-bonding partner in the CD79A TM domain (*SI Appendix*, Fig. S4*D*). The membrane-embedded mIgM-CD79 interface is otherwise dominated by hydrophobic complementarity between the composite mIgM dimer surface and CD79A. Prominently featured in this interface are close packing interactions with mIgM F8 and F12 (*SI Appendix*, Fig. S4 *D* and *E*), explaining why cysteine substitutions at these positions completely blocked receptor assembly (see Fig. 3) regardless of whether they crosslinked strongly (at F8) or very weakly (at F12). This arrangement is reminiscent of FcεRIγ dimer assembly with several different Fc receptor α-chains (33), wherein a YxxxxT motif stabilizes the FcεRIγ dimer on one side and opens to engage alternative polar contacts to α-chains on the other side. Interestingly, the cryo-EM structures also reveal that one mIgM heavy chain linker region passes through the space between CD79A and CD79B linker regions just above the TM domains (36, 37), intertwining the disulfide-linked mIgM and CD79 dimers in a way that is only possible through the cooperative and cotranslational ER assembly that is evidenced by our mixing control shown in Fig. 2*A*. This arrangement makes it all the more surprising that apparently mild mutations like serine to valine in the mIgM TM dimer interface can cause a near-complete dissolution or block in assembly of the BCR complex (see Fig. 5).

The BCR now joins a growing list of immune signaling proteins that feature the YxxxxT motif in TM interfaces. These include TCRαβ, TCRγδ, and pre-TCR heterodimers (9, 18, 20), where the tyrosine and threonine are on different chains and therefore do not constitute a linear sequence motif, as well as the homodimeric complexes formed by the TCR-associated ζ chain (32), FcεRIγ (33), and CD28 and CTLA-4 (34), where the linear motif is readily apparent in sequence alignments (see Fig. 6*C*). With the added examples of all the five BCR mIg isotypes, we can now refine this interaction motif to Y(sm)xxxT because all of the homodimeric proteins and TCRβ sequences contain a small amino acid (glycine, alanine, or serine) directly following the tyrosine. The interactions mediated by this motif have both established and hypothetical functional significance in several different scenarios. For example, in CD28, the dimerization potential of the YxxxxT motif was reported to be comparable to that of glycophorin A's GxxxG motif (34, 54, 55), the most common benchmark in TM helix dimerization. This has immediate clinical implications, because CD28 TM domains are used in chimeric antigen receptors (CARs) for cancer immunotherapy (56, 57), where the YxxxxT motif drives unintended interactions between CARs and endogenous CD28 in patient T cells (35, 58) and may thereby contribute to enhanced function (59) and/or toxicity (57).

The observation that all types of T cell and B cell antigen receptors use similar dimeric structures at the core of their TM assemblies indicates that this arrangement confers favorable properties. This may be as simple as providing stability in the membrane to maintain receptor complex integrity during interactions with polymeric and cell-bound antigens that exert mechanical forces. Such forces have been proposed to regulate TCR and BCR activation (60–63) through mechanisms that could involve conformational changes propagating through the membrane-embedded structures. However, not all TCR studies support this type of mechanism (see

for example refs. 64–66), and equally plausible activation models exist for both TCR and BCR that do not invoke allosteric changes, force induced or otherwise (43, 44, 67, 68). Additionally, cholesterol binds directly to the TCR in the membrane in a way that is reported to regulate function (69–72), and two recent cryo-EM structures show that a large part of the cholesterol-binding site is formed by the composite surface of the TCRαβ core TM structure (66, 73). Structural alterations and increased dynamics in this region have been suggested to accompany active signaling (73–75), suggesting a complex interplay among TM interactions, cholesterol binding, and signal propagation. How interactions with cholesterol may regulate the BCR is less well studied. To the extent that evaluating different receptor activation models depends on specific structural information within the membrane, identification of the shared core TM structure described here now provides a basis for structurally informed hypothesis testing in cellular systems.

Methods

Experimental Methods.

Genes and constructs. The HyHEL10-specific mouse mIgM heavy chain and κ light chain genes were synthesized as gene blocks by Integrated DNA Technologies (full sequences in supplement). For the mouse CD79A and B genes, total B cell mRNA kindly provided by the Hodgkin Lab (WEHI) was first reverse transcribed to cDNA using SuperScript™ III Reverse Transcriptase (Invitrogen). Primers specific to the native N- and C-terminal sequences of CD79 A/B (listed in supplement) were used to generate CD79A/B DNA fragments by PCR. Each BCR chain gene fragment was cloned into pSP64 poly(A) backbone vector (Promega) by restriction–ligation using HindIII and BamHI (New England BioLabs). Affinity tags (HA/SBP/FLAG) were encoded C-terminal to the BCR chains, separated by a GS or GSG linker. All mutations were generated by QuickChange (Agilent) site-directed mutagenesis following manufacturer's instructions.

In vitro BCR assembly. In vitro BCR assembly was performed using rabbit reticulocyte lysate in vitro translation (IVT) system and amino acid mixture minus methionine and cysteine (Promega). ^{35}S-labeled methionine and cysteine (Perkin Elmer) were added to visualize results by autoradiography. The IVT system was supplemented with ER microsomes purified from IVD12 cells (16, 76) to support native membrane protein assembly. Template mRNA for the IVT system was generated using the RiboMAX T7 Large-Scale RNA Production kit (Promega). Per 25 uL IVT reaction, approximately 200 ng HC and 75 ng of CD79A and B mRNA were added, with small adjustments made to equalize translation between mutants and/or mRNA preparations. Total mRNA content per reaction never exceeded 500 ng. The BCR subunits were translated for 30 min at 30°C, and then gentle oxidizing conditions were introduced to support protein folding by the addition of 2 mM oxidized glutathione (GSSG) and reduced glutathione (GSH). The complexes were assembled for another 4 h at 30°C. Assembly reactions were stopped by the addition of 900 uL phosphate-buffered saline (PBS) and centrifuged to pellet the ER microsomes. For the cysteine crosslinking reactions, IVT was stopped by the addition of 500 uL PBS containing 2 mM CuPhe (from a stock containing 100 mM o-phenanthroline and 30 mM $CuSO_4$ in 20% ethanol) to catalyze transmembrane disulfide bond formation, and the reactions were frozen overnight, thawed at 30°C for 30 min, and then centrifuged. BCR complexes were extracted from the ER microsome pellet at 4°C for 1 h using 0.5% digitonin in PBS containing 100 μg/ml BSA and 10 mM iodoacetamide to prevent disulfide bond formation at subsequent steps, followed by centrifugation through a Spin-X tube (Sigma) to remove insoluble material. Immunoprecipitations were done at 4°C for 2 h or overnight using mouse anti-FLAG M2-agarose, streptavidin–agarose, or mouse anti-HA-agarose (clone HA-7) (all from Sigma). For the SBP->HA sequential nondenaturing immunoprecipitations (snIPs), after the first IP with streptavidin–agarose, samples were incubated with biotin for 30 min and then passed through a Spin-X centrifuge tube (to remove the streptavidin–agarose beads) and immunoprecipitated with anti-HA agarose. Following IP, the samples were deglycosylated with Endo H or Hf (NEB), and SDS-PAGE was performed in 4 to 12% Bis-Tris gels (Life Technologies) and 3-(N-morpholino)propanesulfonic acid running buffer (Thermo Fisher Scientific). Gels were then transferred onto polyvinylidene fluoride membranes and exposed to a tritium screen overnight to read the results by phosphorimaging.

Computational Methods.

Mouse mIgM TM assembly modeling in implicit bilayer. To model the mouse mIgM TM homodimer structures, replica exchange molecular dynamics (REMD) simulations (77) with experimentally derived distance restraints (experimentally guided REMD) in an implicit membrane were employed, which has been demonstrated to be effective for TCR TM assembly (18, 19). In terms of efficiency of conformational sampling of TM assembly, REMD in an implicit membrane model is (practically) equivalent to the replica exchange with solute scaling (REST2) (78) in which only the interactions between peptides and proteins are scaled for the facilitated sampling of their conformations. Because there exists no explicit solvent, the conformations of TM assembly may be sampled more efficiently. Regarding the computational costs, the experimentally guided REMD can be an order of magnitude more efficient than conventional REMD. With experimentally derived distance restraints, an accurately converged structure model of TCR TM assembly was obtained from only several ns REMD simulations (18). Without these restraints, it could take much longer to obtain well-converged structure model, if possible. For example, a 110-ns conventional REMD simulation in an implicit membrane was required to obtain a converged structure model of CD247 dimer and CD61A complex (33).

The mouse mIgM TM domain (sequence: ENLWTTASTFIVLFLLSLFYSTTVTLFKVK) was initially modeled as a helix, with the principal axis of each mIgM TM helix initially aligned along the membrane normal (z-redirection). An REMD system was composed of 44 replicas in a temperature range of 300–900 K, where the two mIgM TM helices were initially separated by 30 Å with random orientations (rotations along each principal axis). To prevent (possible) helix unfolding at high temperatures, weak dihedral restraints were applied along φ and ψ angles for the residues in the TM domain. A 7-ns Langevin dynamics REMD simulation was performed in the GBSW implicit membrane model (47) using CHARMM (48), where the collision frequency for Langevin dynamics was set to $\gamma = 5$ ps^{-1} and the GBSW default options provided in Implicit Solvent Modeler in CHARMM-Graphic User Interface (GUI) (79) were used with an empirical surface tension coefficient (0.03 kcal/mol/Å^2) for the nonpolar solvation contribution. For three residue pairs identified in cysteine scanning experiments (L1, A5, and S19), distance restraints were applied between Cβ atoms of each pair, where the CHARMM default options for Nuclear Overhauser effect (NOE) restraints with a soft asymptote were used with RMIN = 3.7 Å and RMAX = 6.0 Å. The integration time step was

set to 2 fs with SHAKE algorithm (80) for constraining covalent bonds involving hydrogen atoms. Replica exchanges were attempted every 1 ps, controlled by the CHARMM REPDSTR module (81). The centroid structure obtained from the cluster analysis (see below) was used to model the initial structures of mIgM and additional four isotypes (mIgD, mIgG, mIgA, and mIgE) in explicit bilayer simulations.

Molecular dynamics simulations in explicit lipid bilayer. The mouse mIgM centroid structure from experimentally guided REMD simulations was inserted into an explicit POPC bilayer using *Membrane Builder* (82). Although a more realistic multicomponent asymmetric bilayer could be considered, to avoid (possible) complications in the generation of an asymmetric bilayer (83), we chose a single-component POPC bilayer as our model membrane because the main purpose of the molecular dynamics simulations was to evaluate the stability of the REMD model in an explicit membrane environment. The system was composed of the TM model with 60 POPC lipids in each leaflet and bulk water with 150 mM KCl. For better statistics, we prepared five independent replicas. The same procedure was repeated for the other four mIg isotypes (mIgD: NGLWPTMCTFVALFLLTLLYSGFVTFIKVK, mIgG: DGLWTTITIFISLFLLSVCYSASVTLFKVK, mIgA: ASLWPTTVTFLTLFLLSLFYSTALTVTTVR, and mIgE: EELWTSICVFITLFLLSVSYGATVTVLKVK). For each prepared system, a series of short constant volume and temperature and constant temperature and pressure (NPT) equilibration runs were performed following the Membrane Builder's six-step protocol (84), followed by a 500-ns restraint-free NPT production run. All simulations were performed using OpenMM (85, 86) with the C36 protein (87) and lipid (88) force fields and TIP3P water model (89, 90), whose integration time step was set to 2 fs with SHAKE algorithm. The van der Waals interactions were smoothly switched off over 10–12 Å by a force-based switching function (91), and the electrostatic interactions were calculated by particle-mesh Ewald method (92). The temperature (T = 300.15 K) and the pressure (p = 1 atm) were controlled by Langevin dynamics with a friction coefficient 1 ps^{-1} and a semi-isotropic Monte Carlo barostat (93, 94) with a pressure coupling frequency of 100 steps, respectively.

Analysis. To evaluate the sampled conformations during distance-restrained REMD, we performed hierarchical clustering, where initially all sample conformations were assigned to different clusters. Starting from these initial clusters, pairs were merged when root mean square deviation between Cα atoms (Cα-RMSD) was less than a cutoff value of 3 Å. The clustering was iterated until there was no cluster closer than the RMSD cutoff. As the Cβ–Cβ distances for the restrained residue pairs converged within the first one ns (except L1–L1 distance, which converged before 3-ns) (Fig. 4*B*), 400 samples were clustered from the 3–7 ns REMD simulation trajectory at T = 300 K, which resulted in a single cluster. For TM models in explicit POPC bilayer, we calculated Cα-RMSD from their initial structure, Cβ–Cβ distances for several residue pairs, inter-TM hydrogen bond occupancy, inter-TM contact probability, Cα–Cα distances for all residue pairs, and the helix–helix distance (d_{HH}) between the two TM helices and their crossing angles (Ω). For a conformation at a given time frame, a hydrogen bond between donor (D) and acceptor (A) atoms is assumed to exist when these atoms are closer than 2.8 Å and the angle formed by D-H···A is greater than 120°. The contact state between a pair of residues is assigned to 1 when the minimum distance between heavy atoms in the residue pair is smaller than 4.5 Å and 0 otherwise. The d_{HH} and Ω were calculated following Chothia et al. (95) d_{HH} is defined as the minimum distance between two helical principal axes that are in turn defined using Cα atoms in the TM domain, and Ω is defined as the dihedral angle between two planes, each defined by the corresponding helical axis and d_{HH} vectors. As the time series of various properties, such as RMSD of TM dimer model, d_{HH}, and Ω (*SI Appendix*, Fig. S2 *B–D*), became steady within 300 ns, the last 200-ns trajectories from each replica were analyzed. For each mIg isotype, the hydrogen bond occupancy, contact probability, the distribution of d_{HH} and Ω, and Cα–Cα distances between residue pairs as a function of Ω were averaged over replicas. Also, representative conformations of mIg TMs in POPC bilayer were obtained from the cluster analysis based on Cα-RMSD between mIg TMs with the same cutoff.

Data, Materials, and Software Availability. All study data are included in the article and/or *SI Appendix*.

ACKNOWLEDGMENTS. This work was supported in part by Australian National Health and Medical Research Council (NHMRC) Infrastructure Support (through the Independent Research Institute Infrastructure Support Scheme, IRIISS), Victorian Government Operational Infrastructure Support (to WEHI), Australian Government Research Training Program Scholarship (to S.R.), and NSF MCB-2111728 (to W.I.).

Author affiliations: [a]Structural Biology Division, The Walter and Eliza Hall Institute of Medical Research, Parkville, VIC 3052, Australia; [b]Department of Medical Biology, The University of Melbourne, Parkville, VIC 3052, Australia; [c]Department of Biological Sciences, Lehigh University, Bethlehem, PA 18015; [d]Department of Bioengineering, Lehigh University, Bethlehem, PA 18015; and [e]Department of Chemistry, Lehigh University, Bethlehem, PA 18015

1. R. Berry, M. E. Call, Modular activating receptors in innate and adaptive immunity. *Biochemistry* **56**, 1383–1402 (2017).
2. M. Reth, Antigen receptor tail clue. *Nature* **338**, 383 (1989).
3. F. W. Alt *et al.*, Synthesis of secreted and membrane-bound immunoglobulin mu heavy chains is directed by mRNAs that differ at their 3′ ends. *Cell* **20**, 293–301 (1980).
4. P. Early *et al.*, Two mRNAs can be produced from a single immunoglobulin mu gene by alternative RNA processing pathways. *Cell* **20**, 313–319 (1980).
5. J. Hombach, T. Tsubata, L. Leclercq, H. Stappert, M. Reth, Molecular components of the B-cell antigen receptor complex of the IgM class. *Nature* **343**, 760–762 (1990).
6. M. Reth, Antigen receptors on B lymphocytes. *Annu. Rev. Immunol.* **10**, 97–121 (1992).
7. D. N. Garboczi *et al.*, Structure of the complex between human T-cell receptor, viral peptide and HLA-A2. *Nature* **384**, 134–141 (1996).
8. K. C. Garcia *et al.*, An alphabeta T cell receptor structure at 2.5 A and its orientation in the TCR-MHC complex. *Science* **274**, 209–219 (1996).
9. Dong *et al.*, Structural basis of assembly of the human T cell receptor-CD3 complex. *Nature* **573**, 546–552 (2019).
10. N. Manolios, J. S. Bonifacino, R. D. Klausner, Transmembrane helical interactions and the assembly of the T cell receptor complex. *Science* **249**, 274–277 (1990).
11. N. Manolios, F. Letourneur, J. S. Bonifacino, R. D. Klausner, Pairwise, cooperative and inhibitory interactions describe the assembly and probable structure of the T-cell antigen receptor. *EMBO J.* **10**, 1643–1651 (1991).
12. P. Cosson, S. P. Lankford, J. S. Bonifacino, R. D. Klausner, Membrane protein association by potential intramembrane charge pairs. *Nature* **351**, 414–416 (1991).
13. T. Rutledge, P. Cosson, N. Manolios, J. S. Bonifacino, R. D. Klausner, Transmembrane helical interactions: Zeta chain dimerization and functional association with the T cell antigen receptor. *EMBO J.* **11**, 3245–3254 (1992).
14. B. Alarcon, B. Berkhout, J. Breitmeyer, C. Terhorst, Assembly of the human T cell receptor-CD3 complex takes place in the endoplasmic reticulum and involves intermediary complexes between the CD3-gamma. delta.epsilon core and single T cell receptor alpha or beta chains. *J. Biol. Chem.* **263**, 2953–2961 (1988).
15. R. S. Blumberg *et al.*, Assembly and function of the T cell antigen receptor. Requirement of either the lysine or arginine residues in the transmembrane region of the alpha chain. *J. Biol. Chem.* **265**, 14036–14043 (1990).
16. M. E. Call, J. Pyrdol, M. Wiedmann, K. W. Wucherpfennig, The organizing principle in the formation of the T cell receptor-CD3 complex. *Cell* **111**, 967–979 (2002).
17. M. E. Call, J. Pyrdol, K. W. Wucherpfennig, Stoichiometry of the T-cell receptor-CD3 complex and key intermediates assembled in the endoplasmic reticulum. *EMBO J.* **23**, 2348–2357 (2004).
18. L. Krshnan, S. Park, W. Im, M. J. Call, M. E. Call, A conserved alphabeta transmembrane interface forms the core of a compact T-cell receptor-CD3 structure within the membrane. *Proc. Natl. Acad. Sci. U.S.A.* **113**, E6649–E6658 (2016).
19. S. Ramesh, S. Park, M. J. Call, W. Im, M. E. Call, Experimentally guided computational methods yield highly accurate insights into transmembrane interactions within the T cell receptor complex. *J. Phys. Chem. B* **124**, 10303–10310 (2020).

20. S. Park, L. Krshnan, M. J. Call, M. E. Call, W. Im, Structural conservation and effects of alterations in T cell receptor transmembrane interfaces. *Biophys J.* **114**, 1030–1035 (2018).
21. K. S. Campbell, B. T. Backstrom, G. Tiefenthaler, E. Palmer, CART: A conserved antigen receptor transmembrane motif. *Semin. Immunol.* **6**, 393–410 (1994).
22. J. H. Blum, T. L. Stevens, A. L. DeFranco, Role of the mu immunoglobulin heavy chain transmembrane and cytoplasmic domains in B cell antigen receptor expression and signal transduction. *J. Biol. Chem.* **268**, 27236–27245 (1993).
23. S. A. Grupp, K. Campbell, R. N. Mitchell, J. C. Cambier, A. K. Abbas, Signaling-defective mutants of the B lymphocyte antigen receptor fail to associate with Ig-alpha and Ig-beta/gamma. *J. Biol. Chem.* **268**, 25776–25779 (1993).
24. C. M. Pleiman, N. C. Chien, J. C. Cambier, Point mutations define a mIgM transmembrane region motif that determines intersubunit signal transduction in the antigen receptor. *J. Immunol.* **152**, 2837–2844 (1994).
25. M. Sanchez *et al.*, Signal transduction by immunoglobulin is mediated through Ig alpha and Ig beta. *J. Exp. Med.* **178**, 1049–1055 (1993).
26. A. C. Shaw *et al.*, Mutations of immunoglobulin transmembrane and cytoplasmic domains: Effects on intracellular signaling and antigen presentation. *Cell* **63**, 381–392 (1990).
27. T. L. Stevens, J. H. Blum, S. P. Foy, L. Matsuuchi, A. L. DeFranco, A mutation of the mu transmembrane that disrupts endoplasmic reticulum retention. Effects on association with accessory proteins and signal transduction. *J. Immunol.* **152**, 4397–4406 (1994).
28. M. D. Friess, K. Pluhackova, R. A. Bockmann, Structural model of the mIgM B-cell receptor transmembrane domain from self-association molecular dynamics simulations. *Front. Immunol.* **9**, 2947 (2018).
29. C. Gottwick *et al.*, A symmetric geometry of transmembrane domains inside the B cell antigen receptor complex. *Proc. Natl. Acad. Sci. U.S.A.* **116**, 13468–13473 (2019).
30. W. W. Schamel, M. Reth, Monomeric and oligomeric complexes of the B cell antigen receptor. *Immunity* **13**, 5–14 (2000).
31. J. Yang, M. Reth, Receptor dissociation and B-cell activation. *Curr. Top. Microbiol. Immunol.* **393**, 27–43 (2016).
32. M. E. Call *et al.*, The structure of the ζζ Transmembrane dimer reveals features essential for its assembly with the T cell receptor. *Cell* **127**, 355–368 (2006).
33. A. Blazquez-Moreno *et al.*, Transmembrane features governing Fc receptor CD16A assembly with CD16A signaling adaptor molecules. *Proc. Natl. Acad. Sci. U.S.A.*, **114**, E5645–e5654 (2017).
34. S. A. Leddon *et al.*, The CD28 transmembrane domain contains an essential dimerization Motif. *Front. Immunol.* **11**, 1519 (2020).
35. Y. D. Muller *et al.*, The CD28-transmembrane domain mediates chimeric antigen receptor heterodimerization with CD28. *Front. Immunol.* **12**, 639818 (2021).
36. X. Ma *et al.*, Cryo-EM structures of two human B cell receptor isotypes. *Science* **377**, 880–885 (2022).
37. Q. Su *et al.*, Cryo-EM structure of the human IgM B cell receptor. *Science* **377**, 875–880 (2022).
38. J. B. Huppa, H. L. Ploegh, In vitro translation and assembly of a complete T cell receptor-CD3 complex. *J. Exp. Med.* **186**, 393–403 (1997).
39. J. Feng, D. Garrity, M. E. Call, H. Moffett, K. W. Wucherpfennig, Convergence on a distinctive assembly mechanism by unrelated families of activating immune receptors. *Immunity* **22**, 427–438 (2005).
40. D. Garrity, M. E. Call, J. Feng, K. W. Wucherpfennig, The activating NKG2D receptor assembles in the membrane with two signaling dimers into a hexameric structure. *Proc. Natl. Acad. Sci. U.S.A.* **102**, 7641–7646 (2005).
41. J. Feng, M. E. Call, K. W. Wucherpfennig, The assembly of diverse immune receptors is focused on a polar membrane-embedded interaction site. *PLoS Biol.* **4**, e142 (2006).
42. K. Tsumoto *et al.*, Contribution to antibody-antigen interaction of structurally perturbed antigenic residues upon antibody binding. *J. Biol. Chem.* **269**, 28777–28782 (1994).
43. P. Tolar, J. Hanna, P. D. Krueger, S. K. Pierce, The constant region of the membrane immunoglobulin mediates B cell-receptor clustering and signaling in response to membrane antigens. *Immunity* **30**, 44–55 (2009).
44. J. Yang, M. Reth, Oligomeric organization of the B-cell antigen receptor on resting cells. *Nature* **467**, 465–469 (2010).
45. P. K. Mattila *et al.*, The actin and tetraspanin networks organize receptor nanoclusters to regulate B cell receptor-mediated signaling. *Immunity* **38**, 461–474 (2013).
46. K. Kläsener, P. C. Maity, E. Hobeika, J. Yang, M. Reth, B cell activation involves nanoscale receptor reorganizations and inside-out signaling by Syk. *eLife* **3**, e02069 (2014).
47. W. Im, M. S. Lee, C. L. Brooks 3rd, Generalized born model with a simple smoothing function. *J. Comput. Chem.* **24**, 1691–1702 (2003).
48. B. R. Brooks *et al.*, CHARMM: The biomolecular simulation program. *J. Comput. Chem.* **30**, 1545–1614 (2009).
49. D. G. Schatz, Y. Ji, Recombination centres and the orchestration of V(D)J recombination. *Nat. Rev. Immunol.* **11**, 251–263 (2011).
50. M. Oettinger, D. Schatz, C. Gorka, D. Baltimore, RAG-1 and RAG-2, adjacent genes that synergistically activate V(D)J recombination. *Science* **248**, 1517–1523 (1990).
51. M. M. Davis, P. J. Bjorkman, T-cell antigen receptor genes and T-cell recognition. *Nature* **334**, 395–402 (1988).
52. S. Tonegawa, Somatic generation of antibody diversity. *Nature* **302**, 575–581 (1983).
53. G. D. Yancopoulos, T. K. Blackwell, H. Suh, L. Hood, F. W. Alt, Introduced T cell receptor variable region gene segments recombine in pre-B cells: Evidence that B and T cells use a common recombinase. *Cell* **44**, 251–259 (1986).
54. M. A. Lemmon *et al.*, Glycophorin A dimerization is driven by specific interactions between transmembrane alpha-helices. *J. Biol. Chem.* **267**, 7683–7689 (1992).
55. K. R. MacKenzie, J. H. Prestegard, D. M. Engelman, A transmembrane helix dimer: structure and implications. *Science* **276**, 131–133 (1997).
56. N. J. Chandler, M. J. Call, M. E. Call, T Cell Activation machinery: Form and function in natural and engineered immune receptors. *Int. J. Mol. Sci.* **21**, 7424–7450 (2020).
57. A. S. Davey, M. E. Call, M. J. Call, The influence of chimeric antigen receptor structural domains on clinical outcomes and associated toxicities. *Cancers (Basel)* **13**, 38 (2020).
58. A. Elazar *et al.*, De novo-designed transmembrane domains tune engineered receptor functions. *eLife* **11**, e75660 (2022).
59. R. G. Majzner *et al.*, Tuning the antigen density requirement for CAR T-cell activity. *Cancer Discov.* **10**, 702–723 (2020).
60. D. K. Das *et al.*, Force-dependent transition in the T-cell receptor β-subunit allosterically regulates peptide discrimination and pMHC bond lifetime. *Proc. Natl. Acad. Sci. U. S. A.* **112**, 1517–1522 (2015).
61. S. T. Kim *et al.*, The alphabeta T cell receptor is an anisotropic mechanosensor. *J. Biol. Chem.* **284**, 31028–31037 (2009).
62. B. Liu, W. Chen, B. D. Evavold, C. Zhu, Accumulation of dynamic catch bonds between TCR and agonist peptide-MHC triggers T cell signaling. *Cell* **157**, 357–368 (2014).
63. Z. Wan *et al.*, The activation of IgM- or isotype-switched IgG- and IgE-BCR exhibits distinct mechanical force sensitivity and threshold. *Elife* **4**, e06925 (2015).
64. J. Gohring *et al.*, Temporal analysis of T-cell receptor-imposed forces via quantitative single molecule FRET measurements. *Nat. Commun.* **12**, 2502 (2021).
65. L. Limozin *et al.*, TCR-pMHC kinetics under force in a cell-free system show no intrinsic catch bond, but a minimal encounter duration before binding. *Proc. Natl. Acad. Sci. U.S.A.* **116**, 16943–16948 (2019).
66. L. Susac *et al.*, Structure of a fully assembled tumor-specific T cell receptor ligated by pMHC. *Cell* **185**, 3201–3213.e3219 (2022).
67. S. J. Davis, P. A. van der Merwe, The kinetic-segregation model: TCR triggering and beyond. *Nat. Ommunol.* **7**, 803–809 (2006).
68. J. Pettmann *et al.*, The discriminatory power of the T cell receptor. *Elife* **10**, e67092 (2021).
69. E. Molnar *et al.*, Cholesterol and sphingomyelin drive ligand-independent T-cell antigen receptor nanoclustering. *J. Biol. Chem.* **287**, 42664–42674 (2012).
70. S. Pathan-Chhatbar *et al.*, Direct regulation of the t cell antigen receptor's activity by cholesterol. *Front. Cell Dev. Biol.* **8**, 615996 (2020).
71. M. Swamy *et al.*, A Cholesterol-based allostery model of T cell receptor phosphorylation. *Immunity* **44**, 1091–1101 (2016).
72. F. Wang, K. Beck-García, C. Zorzin, W. W. Schamel, M. M. Davis, Inhibition of T cell receptor signaling by cholesterol sulfate, a naturally occurring derivative of membrane cholesterol. *Nat. Immunol.* **17**, 844–850 (2016).
73. Y. Chen *et al.*, Cholesterol inhibits TCR signaling by directly restricting TCR-CD3 core tunnel motility. *Mol. Cell* **82**, 1278–1287 (2022).
74. A. L. Lanz *et al.*, Allosteric activation of T cell antigen receptor signaling by quaternary structure relaxation. *Cell Rep.* **36**, 109375 (2021).
75. P. R. Pandey, B. Różycki, R. Lipowsky, T. R. Weikl, Structural variability and concerted motions of the T cell receptor - CD3 complex. *eLife* **10**, e67195 (2021).
76. S. Ramesh, "The transmembrane organisation of the B cell antigen receptor" in *Medical Biology (WEHI)*, (University of Melbourne, 2021).
77. Y. Sugita, Y. Okamoto, Replica-exchange molecular dynamics method for protein folding. *Chem. Phys. Lett.* **314**, 141–151 (1999).
78. L. Wang, R. A. Friesner, B. J. Berne, Replica exchange with solute scaling: A more efficient version of replica exchange with solute tempering (REST2). *J. Phys. Chem. B* **115**, 9431–9438 (2011).
79. S. Jo, T. Kim, V. G. Iyer, W. Im, CHARMM-GUI: A web-based graphical user interface for CHARMM. *J. Comput. Chem.* **29**, 1859–1865 (2008).
80. J.-P. Ryckaert, G. Ciccotti, H. J. C. Berendsen, Numerical integration of the cartesian equations of motion of a system with constraints: Molecular dynamics of n-alkanes. *J. Comput. Phys.* **23**, 327–341 (1977).
81. H. L. Woodcock 3rd, *et al.*, Interfacing Q-Chem and CHARMM to perform QM/MM reaction path calculations. *J. Comput. Chem.* **28**, 1485–1502 (2007).
82. E. L. Wu *et al.*, CHARMM-GUI membrane builder toward realistic biological membrane simulations. *J. Comput. Chem.* **35**, 1997–2004 (2014).
83. S. Park, W. Im, R. W. Pastor, Developing initial conditions for simulations of asymmetric membranes: A practical recommendation. *Biophys J.* **120**, 5041–5059 (2021).
84. S. Jo, T. Kim, W. Im, Automated builder and database of protein/membrane complexes for molecular dynamics simulations. *PLoS One* **2**, e880 (2007).
85. P. Eastman *et al.*, OpenMM 7: Rapid development of high performance algorithms for molecular dynamics. *PLoS Comput. Biol.* **13**, e1005659 (2017).
86. J. Lee *et al.*, CHARMM-GUI input generator for NAMD, GROMACS, AMBER, OpenMM, and CHARMM/OpenMM simulations using the CHARMM36 additive force field. *J. Chem. Theory Comput.* **12**, 405–413 (2016).
87. J. Huang, A. D. MacKerell Jr, CHARMM36 all-atom additive protein force field: Validation based on comparison to NMR data. *J. Comput. Chem.* **34**, 2135–2145 (2013).
88. J. B. Klauda *et al.*, Update of the CHARMM all-atom additive force field for lipids: Validation on six lipid types. *J. Phys. Chem. B.* **114**, 7830–7843 (2010).
89. W. L. Jorgensen, J. Chandrasekhar, J. D. Madura, R. W. Impey, M. L. Klein, Comparison of simple potential functions for simulating liquid water. *J. Chem. Phys.* **79**, 926–935 (1983).
90. A. D. MacKerell *et al.*, All-atom empirical potential for molecular modeling and dynamics studies of proteins. *J. Phys. Chem. B.* **102**, 3586–3616 (1998).
91. P. J. Steinbach, B. R. Brooks, New spherical-cutoff methods for long-range forces in macromolecular simulation. *J. Comput. Chem.* **15**, 667–683 (1994).
92. U. Essmann *et al.*, A smooth particle mesh Ewald method. *J. Chem. Phys.* **103**, 8577–8593 (1995).
93. K.-H. Chow, D. M. Ferguson, Isothermal-isobaric molecular dynamics simulations with Monte Carlo volume sampling. *Comput. Phys. Commun.* **91**, 283–289 (1995).
94. J. Åqvist, P. Wennerström, M. Nervall, S. Bjelic, B. O. Brandsdal, Molecular dynamics simulations of water and biomolecules with a Monte Carlo constant pressure algorithm. *Chem. Phys. Lett.* **384**, 288–294 (2004).
95. C. Chothia, M. Levitt, D. Richardson, Helix to helix packing in proteins. *J. Mol. Biol.* **145**, 215–250 (1981).